LOAD COEFFICIENTS AND DIMENSIONS OF RASCHEL KNITTED NETTING MATERIALS IN FISH FARMS

Heidi Moe Føre[1], Per Christian Endresen, Hans V. Bjelland
EXPOSED Aquaculture Research Centre
SINTEF Ocean
Trondheim, Norway

ABSTRACT

New types of fish farms are often larger and structurally more complex than conventional fish farming structures, and associated challenges concerning safety and costs increase correspondingly. Thus, increased precision in structural design is required, with estimation of hydrodynamic loads on nets as an important topic. Today, both load coefficients for nets and measured netting dimensions are given with relatively high uncertainties. New knowledge for netting materials with high solidities as well as scaled netting commonly applied in model tests are included in the presented study. Results from towing tests and the development of a new mathematical expression for local drag coefficients (for netting twines) indicate that drag coefficients are not only dependent on solidity and Reynolds number, but may also be affected by the velocity reduction and the local velocity at the twines.

Keywords: Aquaculture, towing tests, nets, drag coefficient, reduced velocity

NOMENCLATURE

A	area of netting rectangle, equal to $B \cdot H$
A_p	projected netting area, equal to $A \cdot Sn$ (area of netting rectangle multiplied by the solidity)
B	breadth of netting rectangle, inner breadth of frame (horizontal)
C_D	drag coefficient
C_L	lift coefficient
C_d	local drag coefficient for projected netting area
C_l	local lift coefficient for projected netting area
F_D	drag force (horizontal load component)
F_L	lift force (vertical load component)
H	height of netting rectangle, inner height of frame (vertical at zero rotation angle, θ = 0)
K	knot factor; the relationship between measured solidity (Sn_m) and the cylinder solidity (Sn_c). A measure of increased solidity due to increased thickness at knot.
ν	kinematic viscosity (10^{-6} m^2/s)
ρ	water density (998 kg/m^3)
r	velocity reduction factor, $r = U_r/U$
Rn	Reynolds number
s	mesh side
Sn	solidity of netting; the relationship between projected area of the netting material and the total area of the net panel
Sn_c	solidity of netting, assuming that the net may be represented by cylinders crossing each other with no extra material in the joints
Sn_e	solidity of netting, estimated as $2 \cdot t/s$
Sn_m	solidity of netting, measured by digital image analysis
t	twine thickness (measured at twine centre over 1/3 of the mesh side)
θ	rotation angle (panel rotation about y-axis)
U	towing velocity
U_r	reduced relative flow velocity behind the panel
U_n	average relative flow velocity acting on the net
U_t	average relative flow velocity through the meshes of the net

[1] Contact author: heidi.moe.fore@sintef.no

INTRODUCTION

The aquaculture industry is moving towards the use of larger and more complex structures, often situated at locations more exposed to loads from the sea environment than current fish farms [1, 2]. This expansion is driven by an increased demand for farmed fish worldwide and limited space available in near-shore and sheltered locations for fish farming. New types of fish farms are often larger and structurally more complex than conventional fish farming structures, and the associated costs increase correspondingly. Thus, increased precision in structural design is required, as over-dimensioning will involve high costs related to both production, operation and maintenance. At the same time, insufficient structural strength and behavior of fish farms may lead to structural failure, challenges regarding safety and working conditions, and consequently severe accidents affecting both wildlife and personnel.

It is thus essential to be able to precisely estimate hydrodynamic loads on nets to assure a cost effective and optimal design of fish farms. The environmental loads acting on a traditional fish farm are mainly due to hydrodynamic forces acting on the fish enclosure made of netting materials and ropes. These loads are transferred to the mooring system through the floater. The fish enclosure, or net, is usually large to accommodate hundreds of thousands of fish: In industrial marine aquaculture, a volume of about 50.000 m^3 is common for an undeformed net. The net must be an efficient barrier preventing fish from escaping while also facilitating adequate exchange of water in the pen. Calculation of the hydrodynamic loads on nets depend on established load coefficients and the netting solidity. Today, both load coefficients for nets and measured netting dimensions are given with relatively high uncertainties.

Model tests are often applied to study loads and response of new fish farming concepts and to validate and support numerical analysis [3-5]. Scaling of netting materials is challenging as local netting dimensions are very small, with twine thickness and mesh size in the range of millimeters [5]. In addition to the practical challenges in acquiring scaled dimensions of the netting material, reduced dimensions may affect the local flow regime (quantified by Reynolds number) and thus the drag coefficients [6]. Therefore, netting is often scaled by a lower factor than the main dimensions of the structure. More knowledge on load coefficient and hydrodynamic loads on scaled netting materials is needed to improve precision in model test results.

Drag coefficients based on towing tests of full-scale netting materials have been published in several papers [7-13]. These results are consistent for relatively low solidity ratios [13], but for solidities above 0.22, the data is limited and inconsistent [13]. One explanation for this can be that the estimated solidity of the netting may be inaccurate [13]. During structural analysis of fish farms, the solidity of the net should be increased by a factor of 50 % to account for biofouling [14]. It is common to assume that this increased solidity yields a similar increase in drag coefficient as an evenly increased diameter of a netting twine. Thus, it is drag coefficients for relatively high solidity netting materials that is of most interest in strength analysis. All in all, this brings up a need for more knowledge on drag coefficients of high solidity netting materials. Most commercial nets used in Norwegian fish farming has a solidity in the range of 0.15-0.30. Adding biofouling, the structural analysis must account for solidities of 0.22-0.45, which correspond to the mentioned area of scarce and inconsistent existing data.

This paper presents new knowledge on drag and lift coefficients for aquaculture nets acquired through towing tests of net panels, complementing and extending previous work presented in [13]. Both new knowledge for netting materials with high solidities and scaled netting commonly applied in model tests are included in the presented study. The results are compared with similar data from previous studies, and form a basis for new load coefficient models. The paper also includes an assessment of methods for measurement of netting dimensions and solidity. Solidity is the net parameter with most influence on drag coefficients for nets and is thus the most important parameter in load coefficient estimation.

MATERIALS AND METHODS

Netting materials

Four different netting materials were tested in April 2020 (Figure 1), complementing tests performed in 2019 [13]. In total 8 netting panels, i.e. netting rectangles sewn to a steel frame, were tested with the same set-up. The netting materials has been named by their measured solidity (Sn_m) and year of test as N-Sn_m-*a/b*, where *a* represent the year 2020 and *b* 2019 (Table 1). In 2019, netting materials were chosen to represent the range of solidities in conventional fish cages (N18b, N20b and N26b), and in addition a high solidity net were included (N33b), which may represent a conventional netting with biofouling. In 2020, two more nets with high solidities were tested to provide more data for high solidities (N33a and N36a). In addition, two netting materials used in scaled models of nets and net structures were included to investigate whether downscaled netting dimensions may affect the drag coefficients.

All tested nets consisted of Raschel knitted PA6 multifilaments. Various knitting patterns were applied (shown in Figure 2 and Figure 3);

- N33a, N36a, N18b, N20b, N26b: Conventional Raschel knitted netting with a super knot structure (R3s). These netting materials were knitted using three bundles of multifilaments to create one twine. The knot area is strengthened to reduce risk of laddering, involving extra lengths of filaments and consequently increased projected knot area.
- N19a and N26a: Raschel netting with two bundles of filaments building each twine (R2) and a relatively small knot area.
- N33b: Raschel knitted netting with three bundles of multifilaments in each twine (R3). The knot is longer and thinner than the super knot (diagonal to the mesh), and has a pattern that involves use of less filaments than the super knot structure.

Table 1 gives the dimensions of the various netting materials after they have been mounted in a steel frame (see set-up description) measured by hand according to the current industry standard. All measurements were done on wetted netting. Mesh side is found as the distance between two adjacent knots when the netting is stretched with light hand force to form square meshes [14]. The half mesh was obtained by dividing the inner dimensions of the test frame, B and H, with the number of meshes horizontally and vertically in the net panel. The twine diameter was measured using a slide caliper, attempting to not compress the twine during measuring.

Figure 1 shows images of the nets tested in 2020. It can be seen that the local geometry of these materials varies. N19a and N26a both have fairly uniform twine thickness and a relatively small knot area. On the other hand, N36a have a twine thickness that varies over the twine and a complex local geometry. It was difficult to measure the thickness of this netting with a slide caliper, as the results were different depending on where the measurement was made. Thus, the twine thickness given in Table 1 was set as the thickness measured with digital image analysis (Table 2). N33a have a more uniform twine thickness compared to N36a, while the knot areas are quite large compared to the twine thickness.

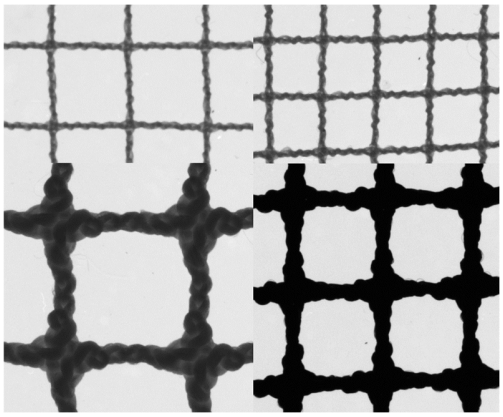

Figure 1: Images of all nets tested in 2020.Top left: N19a. Top right: N26a. Bottom left: N33a. Bottom right: N36a. The nets relative dimensions are approximately preserved.

Solidity measurements

Solidity (Sn) is defined as the relationship between projected area of the netting material and the total area of the net panel [1]. It is given as a number between 0 and 1, where 0 represent no netting material and 1 represent a solid fabric. According to Moe et al. [15], most commercial nets used in Norwegian fish farming has a solidity in the range of 0.15-0.30, with a twine thickness around 2 mm and a mesh side of 10-35 mm (Figure 2, Table 1).

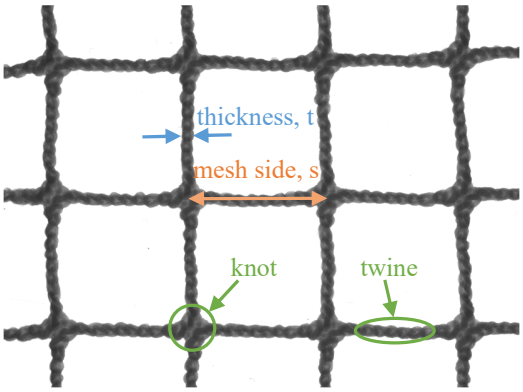

Figure 2: Conventional Raschel knitted netting material for aquaculture with super knot structure (N20b, R3s). Netting dimensions (thickness and mesh side) is indicated. Picture of right side of backlit netting from measurement rig.

Various methods have been applied to quantify netting solidity. In the Norwegian aquaculture industry, it is most common to estimate the solidity (Sn_e) as two times the twine thickness (t) divided by the mesh side (s), as given in eq. 1. The netting is by this considered built up of perfectly square meshes with a constant twine thickness, with extra material at the knot equal to an area of the thickness squared. Dimensions are found by manual measurements applying slide caliper and ruler.

$$Sn_e = 2 \cdot t/s \quad (1)$$

Unfortunately, such estimates are often subjective and inaccurate. Due to the very flexible nature of knitted netting, it is difficult to measure netting dimensions, as the twine is easily stretched and compressed. In addition, the thickness of a twine will vary along the length of the twine. Methods applied to measure twine thickness and mesh side varies and are often not objective. For instance, using a slide caliper to measure twine thickness may be affected both by the caliper and the person making the measurement. The netting must be stretched to form square meshes, and the way this is done will affect the mesh side measurements.

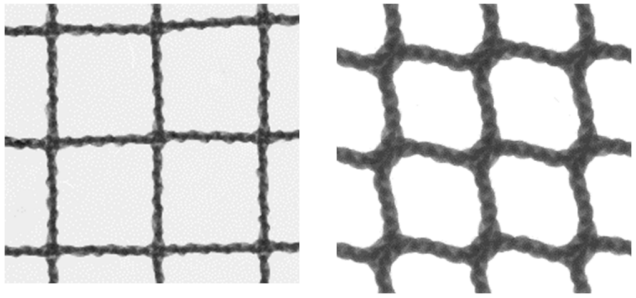

Figure 3: Raschel knitted netting materials with alternative knitting patterns. Left: Netting for scaled models (N19a, R2), and high solidity net (N33b, R3).

Table 1: Netting dimensions measured by hand (slide caliper and ruler) on wet net panels, and estimated solidity (eq. 1).

Netting	Mesh side, s [mm]	Twine thickness, t [mm]	Solidity, Sn_e [-]
N19a	7.8	0.7	0.179
N26a	5.5	0.7	0.255
N33a	13.5	2.0	0.296
N36a	9.0	1.5	0.333
N18b	32.4	2.5	0.15
N20b	27.5	2.2	0.16
N26b	17.3	2.0	0.23
N33b	8.0	1.3	0.32

Table 2: Netting dimensions and solidity measured on wet netting samples by digital image analysis, and calculated knot factor (eq. 2).

Netting	Twine thickness, t [mm]	Solidity, Sn_m [-]	Knot factor, K [-]
N19a	0.7	0.193	1.11
N26a	0.7	0.262	1.09
N33a	2.0	0.331	1.21
N36a	1.5	0.364	1.19
N18b	2.5	0.185	1.23
N20b	2.5	0.199	1.16
N26b	2.0	0.257	1.17
N33b	1.3	0.328	1.08

A measurement rig and software has been developed to ensure objective measurements of solidity, mesh side and twine thickness [16]. The rig consists of a backlit glass plate to support the netting material, and a machine vision camera (FLIR Black Fly S). A piece of netting material is placed on the glass plate and weights are attached to each loose twine to preload the netting. In general, it is recommended that the netting is stretched with a light hand force, equal to approximately 1 N during solidity measurements [16]. However, to measure the solidity of the netting in the net panels, the solidity at the given mesh side during towing tests (Table 1) was sought through applying different loads to the twines. The weights were adjusted for each sample to achieve a mesh side equal to the mesh side measured when the net was attached to the frame during the towing tank tests (60-240 g). Solidity values were fine tuned to the given mesh side (Table 1) by interpolation or extrapolation. The camera was placed approximately 35 cm above the net sample, and a LabVIEW-program was developed for the camera to perform calibrations and processing of the digital images. The program identifies an area of 4 x 4 meshes and calculates solidity as the area covered by netting material divided by the total area (Sn_m) and mesh side (s) based on image pixels. The twine thickness is calculated as the average thickness of the center of each thread over a length equal to one third of the mesh side. Three samples for each net were analyzed (except for N19a where one sample was discarded due to loose fibers disturbing the image analysis), each providing the solidity of 9 meshes, and 24 values for both mesh side and thickness. Measurements presented in Table 2 are the average values of these.

In this work the solidity of the tested net panels was both estimated based on manually measuring mesh side and twine diameter applying eq. 1 (Table 1), and measured through digital image analysis (Table 2). The measured solidity from digital image processing (Sn_m) was applied in post-processing of data from the towing tests, as they gave the most consistent results.

The solidity found from digital image processing (Sn_m) is most often larger than the estimated solidity Sn_e. In commercial netting materials, there is normally additional material in the knot area (Figure 2), which is not fully accounted for when applying eq. 1 to estimate the solidity.

For Raschel knitted netting an increased twine thickness is observed at the joints and will affect the solidity of the netting, particularly for a super-knot structure. In order to quantify this increased projected area, a knot factor (K) is proposed, giving the relationship between the measured solidity (Sn_m) and the cylinder solidity (Sn_c):

$$K = Sn_m/Sn_c \quad (2)$$

Where $Sn_c = 2t/s - (t/s)^2$, based on the assumption that the net may be represented by cylinders crossing each other with no extra material at the knots.

The knot factor of the relevant materials is given in Table 2. It is found that the conventional R3S-netting as expected has a relatively high knot factor, $K \in [1.16,1.23]$, meaning that the strengthened knot area increases the solidity by 16-21% compared to a net with no increased thickness at the knot. Else $K \in [1.08,1.11]$ for the applied netting materials. Sn_m was found to be 2-27 % higher than Sn_e.

Towing test setup and procedure

Towing tests were performed in one of SINTEF Ocean's towing tanks in Trondheim, Norway, known as the ship model tank. This tank is 10.5 m wide and 5.6 m deep, and a length of 175 m was applied in these tests (total length is 260 m). The setup in the towing tank was similar to the setup in [13].

Each net sample was sewn onto a rectangular frame with inner dimensions of 1215 x 985 mm, forming a net panel (Figure 4). The frame was constructed of circular steel pipes with an outer diameter of 16 mm. In addition, two thin steel wires were attached along the diagonals to form a supporting cross behind the netting in order to limit deformation of the netting during towing. The netting was mounted so that the right side of the netting, i.e. the side with V-shaped stitches [13], was facing the towing direction. The net was sewed to the frame using a wetted Nylon twine and occasional cable ties for extra support.

The frame was mounted to the test rig with four 3 DOF load sensors placed on the aft (downstream) side of the frame over the frame height (Figure 5). One of the sensors were clamped in all

axis directions while the others were free to move along the pipe to prevent loads in axial direction of the frame between the grips. The sensors were hinged in different axis directions to prevent internal bending stresses. The submerged part of the test rig consisted mainly of two foil shaped struts situated aft of the net to minimize the impact from the rig on the flow through the panel.

The net panels were towed at constant velocities ranging from 0.1 m/s to 1.75 m/s (in x-direction in Figure 5). Two orientations of the net panel were tested; vertical panels (0°) and panels rotated 45° about the horizontal y-axis (Figure 5). The angle represents the angle between the panel normal vector and the towing direction. The top of the frame was at a depth of approximately 39 cm in vertical position and 47 cm at 45° rotation.

Flow velocity was measured aft of the panel (downstream) up to 1.30 m/s due to the current meter limitations. An electromagnetic current meter was placed at a horizontal distance of 71.5 cm from the net, approximately 90 cm below the water surface in the geometric center of the panel, measuring fluid velocity at this point. Velocity was measured for vertical panels only, as an orientation of 45° interfered with the mounting of the current sensor.

After towing of each net panel, the netting was cut out of the panels, leaving netting residues and seam on the frame. Loads acting on these frames only were measured for all panels and angles, except for N33a at 0° (cancelled due to damage and repair of the rig). In addition, a clean frame where net residues and seems were removed was towed at both angles.

Data processing and presentation

Loads measured by the 4 load sensors during towing include load contributions from the netting, the supportive frame with seams, and grips attaching the frame to the load sensors and test rig (Figure 5). However, it is the loads acting on the netting that are of interest and are published in the Results section. Drag is defined as the force on the panel in the towing direction while lift is a force perpendicular to the drag force. The resulting drag and lift forces acting on the netting only were found by subtracting loads acting on the frame (with grips, steel wires, seams and net residues) from the total measured loads. Since drag loads on the frame of N33a and N36a were similar at 45°, frame drag for N36a at 0° were applied for N33a at 0°.

Forces are presented in Newtons, while dimensionless force coefficients for the netting rectangle were calculated using Eq. 3.

$$C_{D,L} = \frac{2 \cdot F_{D,L}}{\rho \cdot A \cdot U^2} \quad (3)$$

where $C_{D,L}$ is the drag or lift coefficient, $F_{D,L}$ is the corresponding component of the measured load, ρ is the water density (998 kg/m^3), A is the netting area ($B \cdot H$) and U is the relative velocity between panel and water (towing velocity).

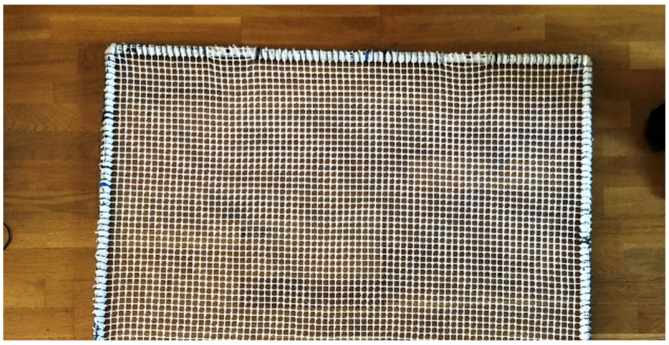

Figure 4: Part of netting panel, netting N33a sewn to the steel pipe frame.

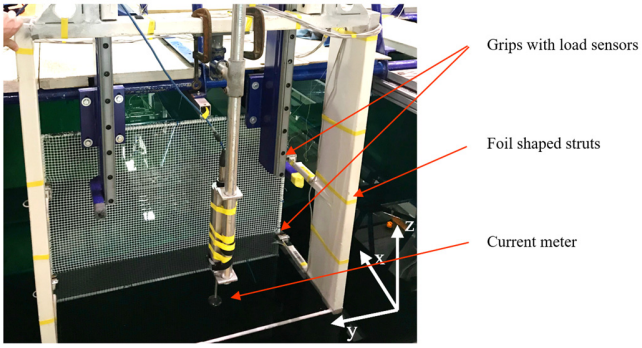

Figure 5: Net panel mounted in test rig with current meter.

Results are also presented as local drag (C_d) and lift coefficients (C_l) for netting twines, using the projected netting area (A_p) as reference, as a function of Reynolds number as given in Eq 3:

$$Rn = \frac{U \cdot t}{\nu} = U \cdot t \cdot 10^6 \, s/m^2 \quad (4)$$

where ν is the kinematic viscosity (10^{-6} m^2/s at 20°C).

Relative velocity measurements behind the panels were applied to estimate how much the netting affected the water flow (wake effects): The velocity reduction factor was calculated as the reduced velocity measured downstream from a panel with netting (U_r) divided by the towing velocity (U) as given in Eq. 5. Velocities measured during testing of frames without netting yielded similar velocities as the towing velocity, and the towing velocity is applied in the presentation of results.

$$r = \frac{U_r}{U} \quad (5)$$

Local drag coefficient as a function of Reynolds number

Kristiansen and Faltinsen [17] derived a model for drag forces on net panels as a function of estimated fluid velocity through the meshes and drag coefficients for individual twines in the netting (assuming a circular cylinder shape [6]). A similar approach was used to investigate the relationship between drag forces, solidity and Reynolds number in the present work.

Considering a net panel with fluid flow perpendicular to the panel ($\theta = 0$), conservation of mass through the panel gives the average fluid velocity through the meshes, U_t, as:

$$U_t = \frac{U}{1 - Sn_m} \tag{6}$$

where U_t and U are the velocities through the mesh and the incident flow to the net panel (towing velocity), respectively.

Kristiansen and Faltinsen [17] found that by using the undisturbed incident velocity U in (eq. 6) to calculate the velocity U_t at the twines, the estimated forces were conservative compared to experiments. They used an alternative formulation for the normal forces on the net based on experimental data [18]. The formula, which is dependent on netting solidity, will in effect reduce the impact on the estimated forces from the calculated local velocity (eq. 6) through the net. Their results thus may indicate that (eq. 6) gives a conservative estimate of the velocity over the twines.

Taylor et al. [19] recounts the current blockage model by Taylor [20], based on the single actuator disc theory by Glauert [21], on the relation between the pressure drop and velocities over an obstacle. Using Bernoulli's equation first upstream and then downstream from the obstruction, [19] presents the pressure drop over the obstruction as a function of the incident flow velocity and the velocity reduction. It was assumed that half of the velocity reduction occurs before the obstruction, while the remaining half of the velocity reduction occurs after (downstream) from the obstruction, resulting in (eq. 7):

$$U_n = \frac{1}{2}(U + U_r) \tag{7}$$

where U_n is the incident velocity acting on the net, and U and U_r are the undisturbed incident flow velocity and velocity in the wake (downstream) respectively. Although the intended use of eq. 7 is for larger obstacles in steady flow, it is applied in the present work to study possible upstream effects on the flow from the net. In the present work the net panel represents the obstruction, and it is assumed that U can be replaced by U_n in eq. 6 to account for the effect of the obstructing net on the incident flow. In addition, the flow reduction factor is applied to express the wake velocity as $U_r = rU$ (eq. 5). Thus, the average flow velocity through the meshes can be described as eq. 8:

$$U_t = \frac{U(1 + r)}{2(1 - Sn_m)} \tag{8}$$

Eq. 8 gives U_t equal to (eq. 6) for $r = 1$, i.e. no net. Decreasing the value of r results in a reduced U_t compared with eq. 6.

Applying U_t (eq. 8) as reference velocity in eq. 3 and dividing the drag coefficient by Sn_m, an equivalent drag coefficient for the projected area of the netting or individual twines (dependent on the undisturbed velocity U), called local drag coefficient C_d, can be expressed as follows (eq. 9):

$$C_d = \frac{F_D}{\frac{1}{2}\rho \cdot A \cdot U^2} \cdot \frac{4(1 - Sn_m)^2}{Sn_m(1 + r)^2} \tag{9}$$

where the first factor on the right-hand side is the drag coefficient C_D based on the area of netting rectangle (A) and the towing velocity (U). Eq. 9 is similar but not equal to the expression derived by Kristiansen and Faltinsen [17].

In [13], describing the test results from 2019, local drag coefficients were presented as C_D/Sn_e (eq. 1). The data set from 2019 yielded similar local drag coefficients for all netting materials independent of solidity, only dependent on net inclination angle to the incident fluid flow and Reynolds number. Tests performed in 2020 did not yield similar results applying C_D/Sn_e. Drag coefficients for tests performed in both 2019 [13] and 2020 are therefore given as local drag coefficients according to (eq. 9) in the present work.

RESULTS

Drag and lift forces

Drag loads on netting for vertical, and inclined net panels and lift loads for a rotation of 45° are given in Figure 6, Figure 7 and Figure 8. Both drag and lift loads acting on the netting increased with increasing velocity, as expected, with maximum values of 416-934N and 102-271N respectively for a towing velocity of 1.75 m/s. The load contribution from the frame has been subtracted from the measured loads. Maximum measured drag forces for the frames (at 1.75 m/s) were in the range of 162-185 N for 0° and 112-133 N for 45°. Values for N19a and N26a were in the lower range and the N33a and N36a in the upper. Drag loads were 19-62% higher than for the clean frame, which yielded 114 N and 97 N for 0° and 45° respectively. Lift loads acting on the frame were small, ranging from 1-5 N.

None of the panels yielded drag loads increasing with velocity squared, as would be expected assuming a constant drag coefficient in eq. 3, indicating that the drag coefficient is not constant in the tested velocity range. For example, if velocity is doubled from 0.5 m/s to 1 m/s, the measured drag load increase with a factor of 3.6-3.8 for the netting rectangles. This indicates that the drag coefficient will vary within the tested range of velocities, i.e. decrease with increasing velocity. The same trend was observed for lift loads.

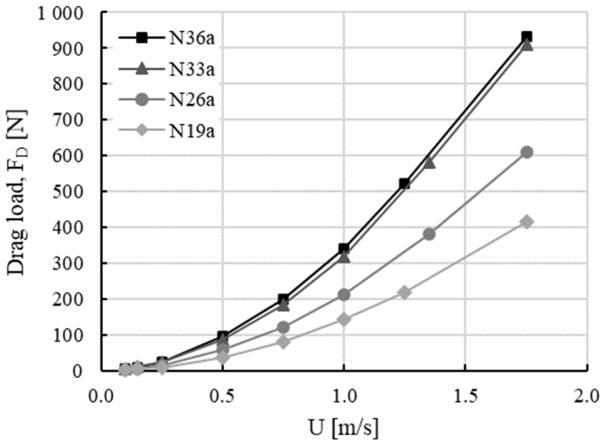

Figure 6: Drag loads on netting in vertical net panels ($\boldsymbol{\theta = 0}$).

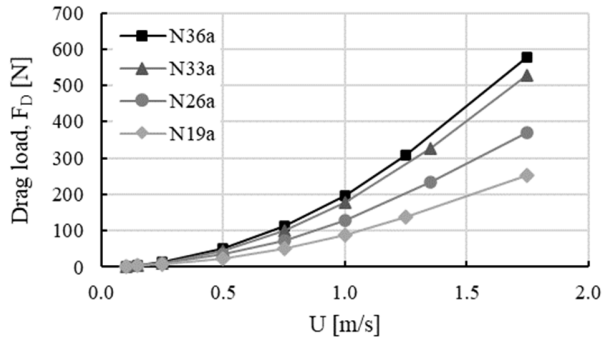

Figure 7: Drag loads on netting in inclined panel ($\boldsymbol{\theta = 45°}$).

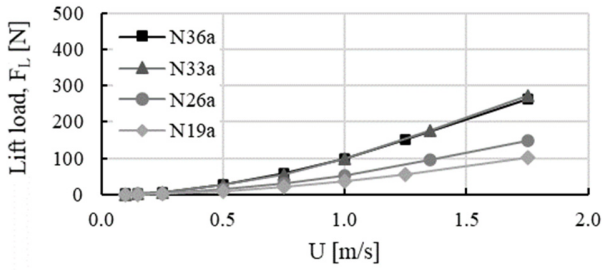

Figure 8: Lift loads on netting in inclined panel ($\boldsymbol{\theta = 45°}$).

Drag and lift coefficients

Drag and lift load coefficients (C_D and C_L) were calculated for the eight netting panels (Table 1 and 2) and different Reynolds numbers (Rn) applying eq. 3. C_D and C_L as a function of measured solidity (Sn_m) for vertical panels and a rotation angle of 45° is given in Figure 9, Figure 10 and Figure 11. 2nd order polynomial trend lines are indicated for Rn = 2000, which in practice for example may represent a 2 mm thick twine subjected to a flow velocity of 1 m/s (eq. 4). The figures show a strong relation between the drag coefficient and the solidity of the netting, and it is found that load coefficients may increase with decreasing Rn. Figure 9 show that load coefficients for a flow velocity of 1 m/s are similar to values given for Rn = 2000.

For a Reynolds number of 2000 and a measured solidity in the range of 0.18-0.36, drag and lift coefficient for netting may be estimated as eq. 10 (polynomials indicated in Figure 9, Figure 10 and Figure 11):

$$C_D(\theta = 0°) = 1.782(Sn_m)^2 + 1.057Sn_m - 0.053 \quad (10)$$
$$C_D(\theta = 45°) = 1.165Sn_m - 0.0919$$
$$C_L(\theta = 45°) = 1.693(Sn_m)^2 - 0.217Sn_m + 0.022$$

Velocity reduction downstream from the net

The velocity reduction factor, r, is given in Figure 12 and Figure 13 as a function of Reynold number and solidity. It was observed that r decreased with increasing solidity, a logical consequence of reduced permeability of the panel. The velocity reduction factor was close to constant for Rn above 1000 for all nets. For Rn lower than 1000, a general trend could not be observed; some nets showed reduces r for reduced Rn, other the opposite. This indicated that for low Rn values, r may depend on other factors than Rn. The cause of this has not been studied but may for instance be different local geometry of the net. It is also important to consider possible errors in velocity measurements for such low velocities.

Figure 13 show that the velocity reduction is highly dependent on the solidity, yielding a linear trend (for $Sn_m \in [0.18, 0.36]$ and $Rn \approx 2000$), given as:

$$r(Sn_m) = 1.08 - 0.97\, Sn_m \quad (11)$$

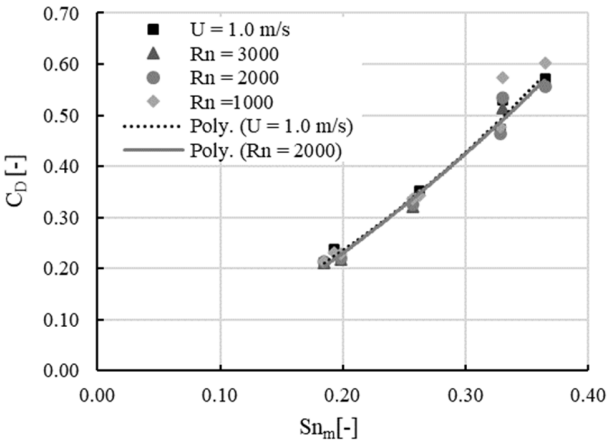

Figure 9: Drag coefficient as a function of measured solidity and Reynolds number for vertical net panels ($\boldsymbol{\theta = 0}$).

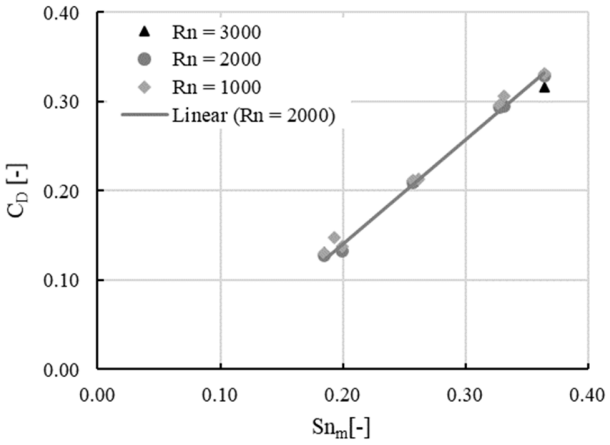

Figure 10: Drag coefficient as a function of measured solidity and Reynolds number for inclined panel ($\boldsymbol{\theta = 45°}$).

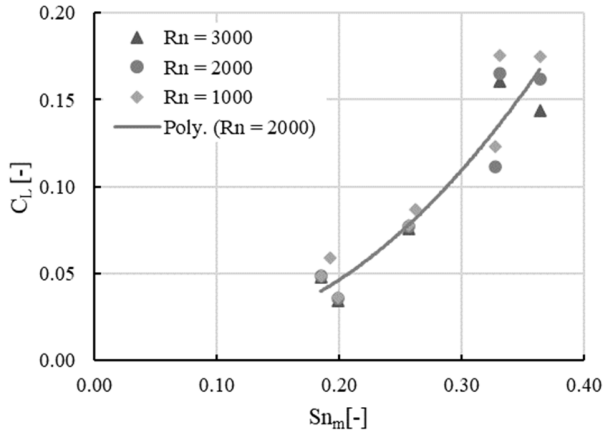

Figure 11: Lift coefficient as a function of measured solidity and Reynolds number for inclined panel ($\boldsymbol{\theta = 45°}$).

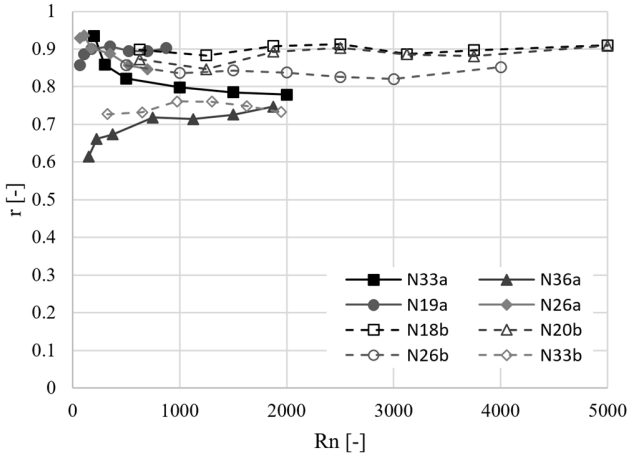

Figure 12: Velocity reduction factor as a function of Reynolds number. Flow perpendicular to the panel ($\boldsymbol{\theta = 0}$).

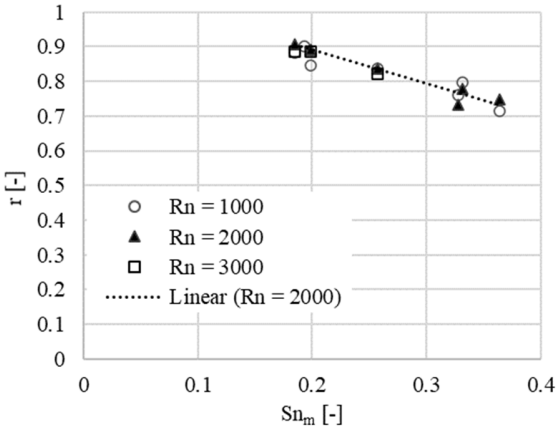

Figure 13: Velocity reduction factor as a function of solidity for tests with Reynolds numbers approximately equal to 1000, 2000 and 3000. Flow perpendicular to the panel ($\boldsymbol{\theta = 0}$).

Local load coefficients

Figure 14 presents the local drag coefficients (C_d) for flow perpendicular to the panel ($\theta = 0°$), which was established applying eq. 9. This required an established flow reduction factor r, and the linear trendline (eq. 11) from Figure 13 was applied to find local load coefficients. The undisturbed incident flow velocity U was used to find the Reynolds number. Applying eq. 9 yields similar drag coefficients for all panels (except N33a), indicating that drag coefficients are not only dependent on solidity and Rn (as found in [13]), but may also be affected by the velocity reduction and the local velocity at the twines. The reason why N33a deviates is not known, but it may be due to the local geometry of the netting.

The results in Figure 14 show a dependency on Reynolds number. Although the results for lowest Rn may very well be affected by error due to the relatively low loads (2-5 N for U = 0.1 m/s), it is probable that the drag coefficient increase with decreasing Rn, in particular below Rn = 500. This trend is supported by established coefficients for a circular cylinder [6]. Generally speaking, the drag coefficient appears close to constant for $Rn > 1500$, with an average value of approximately 0.8. All netting materials show similar C_d for perpendicular flow ($\theta = 0$) and $Rn > 1000$ apart from N33a, which yield a higher drag coefficient than the others. For $Rn < 500$ the difference in drag coefficient between the netting materials increase.

Local drag coefficients (C_d) for flow with a 45-degree angle to the panel ($\theta = 45°$) is given in Figure 15. Although the panels were inclined to the fluid flow, the same method to normalize the drag forces (eq. 9) were used to normalize the drag forces measured for ($\theta = 45°$). This method was chosen although the panel inclination most likely will affect the flow around and through the panel, and thus affect drag forces and coefficients. However, for $\theta = 45°$, this effect is assumed to be small based on findings in [10] and [5], where wake velocity for panels and net cage models with close to 45 degrees inclination were measured. Their results indicated an increase in velocity

reduction with increasing θ, but that the change in wake velocity was relatively small from $\theta = 0$ to $\theta = 30°$ [10] and from $\theta = 0$ to $\theta = 45°$ for [5].

Figure 15 shows a similar trend as drag coefficients for $\theta = 0$. For $Rn > 1000$ the drag coefficients for all inclined nets are close to constant with an approximate value of 0.5. For decreasing Reynolds numbers below 1000 the drag coefficients increase and show larger variations between the netting materials.

Figure 14 and Figure 15 show that both solidity and Reynolds number are parameters that strongly affect the drag coefficient, in addition to the local flow and velocity reduction.

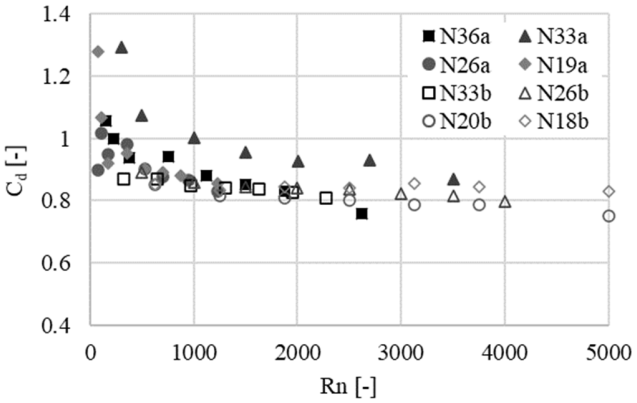

Figure 14: Drag coefficient using twine area and flow velocity through the mesh (eq. 9) plotted as a function of Reynolds number. Flow perpendicular to the panel ($\boldsymbol{\theta = 0}$).

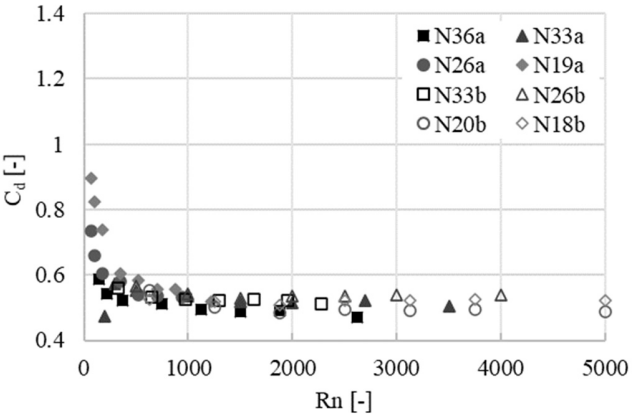

Figure 15: Drag coefficient using twine area and flow velocity through the mesh (eq. 9) plotted as a function of Reynolds number. Inclined panel ($\boldsymbol{\theta = 45°}$).

The lift forces were also normalized using eq. 9, substituting the drag coefficient C_D with the lift coefficient C_L. In contrary to the local drag coefficients (C_d), the local lift coefficient (C_l) for $\theta = 45°$ (Figure 16) in general varied between the different netting materials. Most netting materials yielded lift coefficient steadily decreasing with increasing Reynolds numbers, except N18b and N26b which showed nearly constant C_l for the tested range of Rn. N33a gave the largest lift coefficient, varying between 0.26 and 0.32 and decreasing with increasing Reynolds number, while 20b gave the lowest lift coefficients, also decreasing with increasing Reynolds number and varying between 0.11 and 0.14. The other netting materials, except N36a, had more coincident lift coefficients varying between 0.18 and 0.26. N36a varied between 0.21 to 0.31.

Similar to the drag coefficients, results for the lowest Reynolds numbers are associated with uncertainty due to the relatively low velocities and subsequent small forces measured by the load sensors. This however does not explain the large discrepancies found between the lift coefficients for the different netting materials. One reason may be that solidity and flow velocity are not the only parameters determining lift forces on net panels. The results in Figure 11 show a relation between the lift coefficient (C_L) and solidity, however it is not as clear as for the drag coefficient (C_D) in Figure 10. The local geometry and structure of the twines and knots vary between the different netting materials (Figure 1), including the relative size of the knots, quantified by the knot factor in eq. 2. A relation between the drag forces and the knot factor was sought, but not found. The possible differences in drag and lift characteristics of the twines and knots and between twines and knots may have an effect on the lift forces for the panel, although this seemed not to have a significant effect on the drag coefficient C_d.

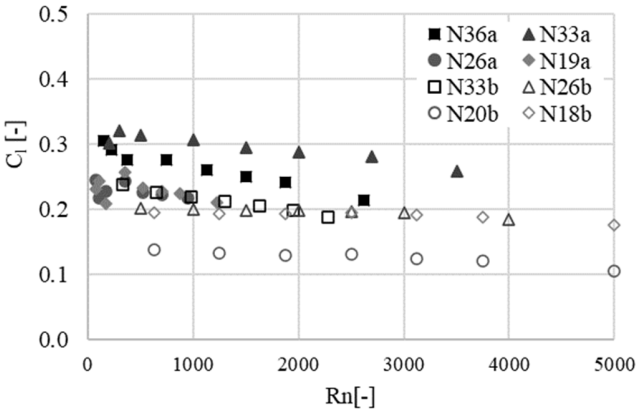

Figure 16: Lift coefficient using twine area and flow velocity through the mesh, similar to the drag coefficient in eq. 9, plotted as a function of Reynolds number. Inclined panel ($\boldsymbol{\theta = 45°}$).

CONCLUSION

Solidity measured with image analysis include the full contribution of the knot area on the solidity, which give the most consistent results in load calculations. This method is also more objective than manual measurements.

Results from towing tests and the development of a new mathematical expression for local drag coefficients (for netting twines), indicate that drag coefficients are dependent on solidity and Reynolds number, but may also be affected by the velocity reduction and the local velocity at the twines. Lift loads were found to vary between the net panels. No consistent general relationship is identified for lift coefficients. Lift may be dependent on local geometry of the netting structure.

Towing test results of in total eight individual netting materials were combined to give load coefficients and velocity reduction factors. The latter were close to proportional to the solidity within the tested solidity range.

ACKNOWLEDGEMENTS

This research has been funded by The Research Council of Norway, EXPOSED Aquaculture Research Centre, grant number 237790. Many thanks to the team at the SINTEF Ocean towing tank for highly skilled work and advice, and the partners of EXPOSED for the good cooperation.

REFERENCES

[1] Chu, Y.I., Wang, C.M., Park, J.C. and Lader, P.F., 2020. Review of cage and containment tank designs for offshore fish farming. Aquaculture.

[2] Bjelland, H.V., Føre, M, Lader, P., Kristiansen, D, Holmen, I.M., Fredheim, A., Grøtli, E.I., Fathi, D.E., Oppedal, F., Utne, I.B., Schjølberg, I., 2015. Exposed aquaculture in Norway: Technologies for robust operations in rough conditions. OCEANS'15 MTS/IEEE Washington, Washington DC, 19-22 October, 2015.

[3] Zhao, Y.-P., Bi, C.-W., Chen, C.-P., Li, Y.-C., Dong, G.-H., 2015. Experimental study on flow velocity and mooring loads for multiple net cages in steady current. Aquacultural Engineering, Volume 67, Pages 24-31, ISSN 0144-8609. https://doi.org/10.1016/j.aquaeng.2015.05.005.

[4] Chun-Wei Bi, Yun-Peng Zhao, Guo-Hai Dong, Yan-Na Zheng, Fu-Kun Gui, 2014. A numerical analysis on the hydrodynamic characteristics of net cages using coupled fluid–structure interaction model, Aquacultural Engineering, Volume 59, Pages 1-12. ISSN 0144-8609. https://doi.org/10.1016/j.aquaeng.2014.01.002.

[5] Moe-Føre, H., Lader, P.F., Lien, E. Hopperstad, O.S., 2016. Structural response of high solidity net cage models in uniform flow. Journal of Fluids and Structures 65, 180-195. 2016.

[6] Schlichting, H., 1968. In: Boundary-LayerTheoryMcGraw-Hill.

[7] Rudi, H., Løland, G. and Furunes, I., 1989. Modellforsøk med nøter. Krefter og gjennomstrømning på enkeltpaneler og merdsystemer. SINTEF Report, Trondheim, Norway. 1989.

[8] Løland, G., 1991. Current forces on and flow through fish farms. PhD thesis, Norwegian Institute of Technology, Division of Marine Hydrodynamics, Trondheim. 1991.

[9] Balash, C., Colbourne, B., Bose, N., Raman-Nair, W., 2009. Aquaculture Net Drag Force and Added Mass. Aquacultural Engineering, Volume 41, Issue 1, Pages 14-21. 2009. ISSN 0144-8609. https://doi.org/10.1016/j.aquaeng.2009.04.003.

[10] Patursson, Ø., Robinson Swift, M., Tsukrov, I., Simonsen, K., Baldwin, K., Fredriksson, D. W., Celikkol, B., 2010. Development of a porous media model with application to flow through and around a net panel. Ocean Engineering, Volume 37, Issues 2–3, Pages 314-324. 2010. ISSN 0029-8018. https://doi.org/10.1016/j.oceaneng.2009.10.001

[11] Gansel, L. C., Jensen, Ø., Lien, E., and Endresen, P. C., 2014. Forces on Nets With Bending Stiffness-An Experimental Study on the Effects of Flow Speed and Angle of Attack. ASME. J. Offshore Mech. Arct. Eng. November 2014. https://doi.org/10.1115/1.4027954.

[12] Zhan, J.M., Jia, X.P., Li, Y.S., Sun, M.G., Guo, G.X., Hu, Y.Z., 2006. Analytical and experimental investigation of drag on nets of fish cages. Aquacultural Engineering, Volume 35, Issue 1, Pages 91-101. 2006. ISSN 144-8609. https://doi.org/10.1016/j.aquaeng.2005.08.013.

[13] Moe Føre, H., Endresen, P.C., Norvik, C., Lader, P., 2021. Hydrodynamic loads on net panels with different solidities. J. Offshore Mech. Arct. Eng. October 2021, Vol. 143 / 051901-1. DOI: 10.1115/1.4049723.

[14] NS 9415.E:2009. Marine fish farms - Requirements for site survey, risk analyses, design, dimensioning, production, installation and operation. Standards Norway. 2009.

[15] Moe, H., Olsen, A., Hopperstad, O. S., Jensen, Ø., Fredheim, A., 2007. Tensile properties for netting materials used in aquaculture net cages. Aquacultural Engineering **37**, 252–265.

[16] Moe Føre, H. and Gaarder, R. H., 2018. RobustNot - Dokumentasjon av mekaniske egenskaper og dimensjoner til notlin i oppdrettsnøter. SINTEF Ocean. SINTEF Ocean report 2018:00971. 2018.

[17] Kristiansen, T., Faltinsen, O. M, 2012. Modelling of current loads on aquaculture net cages. Journal of Fluids and Structures 34, 218-235. 2012.

[18] Blevins, R.D., 2003. Applied Fluid Dynamics Handbook. Krieger Publishing Company, Malabar.

[19] Taylor, P.H., Santo, H., Choo, Y. S, 2013. Current blockage: Reduced Morison forces on space frame structures with high hydrodynamic area, and in regular waves and current. Ocean Engineering 57, 11-24. 2013.

[20] Taylor, P., 1991. Current blockage: reduced forces on offshore space-frame structures. In: Offshore Technology Conference, OTC 6519.

[21] Glauert, H., 1983. The Elements of Aerofoil and Airscrew Theory. Cambridge University Press, Cambridge (1983)